# An Introduction to Atmospheric Radiation

K. N. LIOU

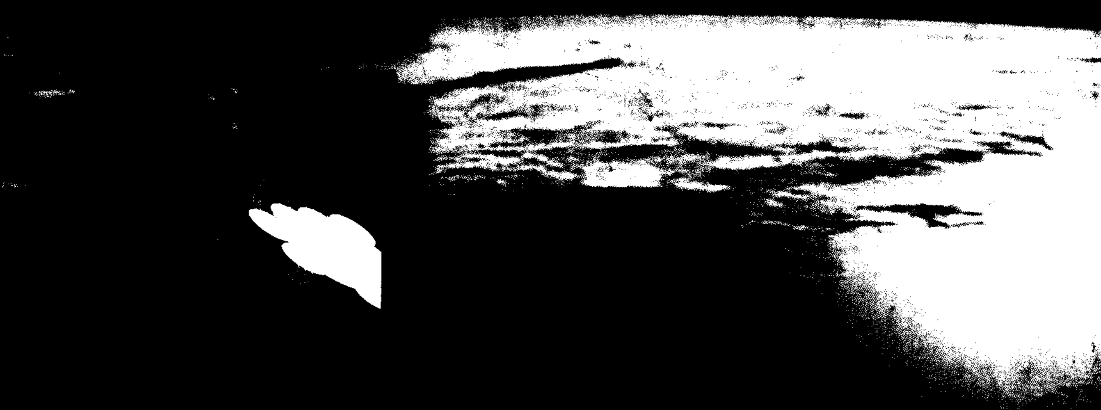

AP INTERNATIONAL GEOPHYSICS SERIES, VOLUME 84

The annual global insolation is proportional to $(1 + e^2/2)$, but is independent of the declination of the sun $\delta$ and the true anomaly $\nu$.

## 2.3 Solar Spectrum and Solar Constant Determination

### 2.3.1 Solar Spectrum

The solar spectrum covers wavelengths ranging from gamma rays to radio waves, as shown in Fig. 1.1. Because of the nonquantized electronic transitions, most solar energy is carried by the continuum, i.e., radiation is continuous rather than selective. The single most important contributor is hydrogen, both in its neutral state and as negative ions. A radiation transition from one level to another is characterized by an absorption or an emission line whose frequency is governed by Planck's relation. However, in the ionization process the atom (or molecules) may absorb more than the minimum energy required to remove the electron. This additional energy may be thought of as supplying kinetic energy to the freed electron and is not quantized. As a consequence, absorption is not selective but rather continuous. The ionization continuum occurs on the high-frequency (shorter wavelength) side of the ionization frequency. Neutral hydrogen has ionization continua associated with lines, some of which were defined in Fig. 1.9. Metallic atoms also contribute to the continuum in the ultraviolet spectrum. The continuum absorption in the visible and infrared spectrum, however, is produced by negative hydrogen ions.

Electromagnetic radiation emerging from within the sun is continuously emitted and absorbed by atoms. As shown in Fig. 2.2, the radiative temperature first drops off to a minimum value of about 4500 K just above the photosphere, and then levels off and slowly rises in the chromosphere, followed by a rapid rise in the transition region to several million degrees in the corona. At each temperature, probabilities of the electronic transition exist that any atom will achieve a particular excited state, leading to the formation of absorption lines at different levels in the solar atmosphere. The core of a line forms at the temperature where the maximum transition probabilities of an electron moving from one orbital level to another occur (see Fig. 1.8). The wings of a line form at different temperature levels because of the required transition probabilities. Each absorption line has a preferred formation region in the solar atmosphere. Those lines that absorb very little radiation are known as weak lines, which can form in narrow layers of the solar atmosphere. Some of the absorption lines in the solar atmosphere were displayed in Fig. 2.2.

In view of the preceding discussion, the solar spectrum consists of a continuous emission with a superimposed line structure. The visible and infrared spectrum of the photosphere shows absorption lines, known as the *Fraunhofer spectrum*. The strongest of these lines are produced by H, Mg, Fe, Ca, and Si, as well as singly ionized Ca and Mg. Most of the lines shorter than 1850 Å produced from the photosphere exhibit in emission. Light from the chromosphere and the corona has emission lines at all observed wavelengths.

2), but is independent of the

**mination**

gamma rays to radio waves,
tronic transitions, most solar
tinuous rather than selective.
th in its neutral state and as
another is characterized by
overned by Planck's relation.
cules) may absorb more than
This additional energy may
electron and is not quantized.
er continuous. The ionization
length) side of the ionization
ssociated with lines, some of
tribute to the continuum in the
visible and infrared spectrum,

e sun is continuously emitted
iative temperature first drops
photosphere, and then levels
a rapid rise in the transition
n temperature, probabilities of
eve a particular excited state,
levels in the solar atmosphere.
maximum transition probabili-
other occur (see Fig. 1.8). The
ause of the required transition
ation region in the solar atmo-
e known as weak lines, which
ome of the absorption lines in

trum consists of a continuous
le and infrared spectrum of the
*nhofer spectrum*. The strongest
s well as singly ionized Ca and
from the photosphere exhibit
rona has emission lines at all



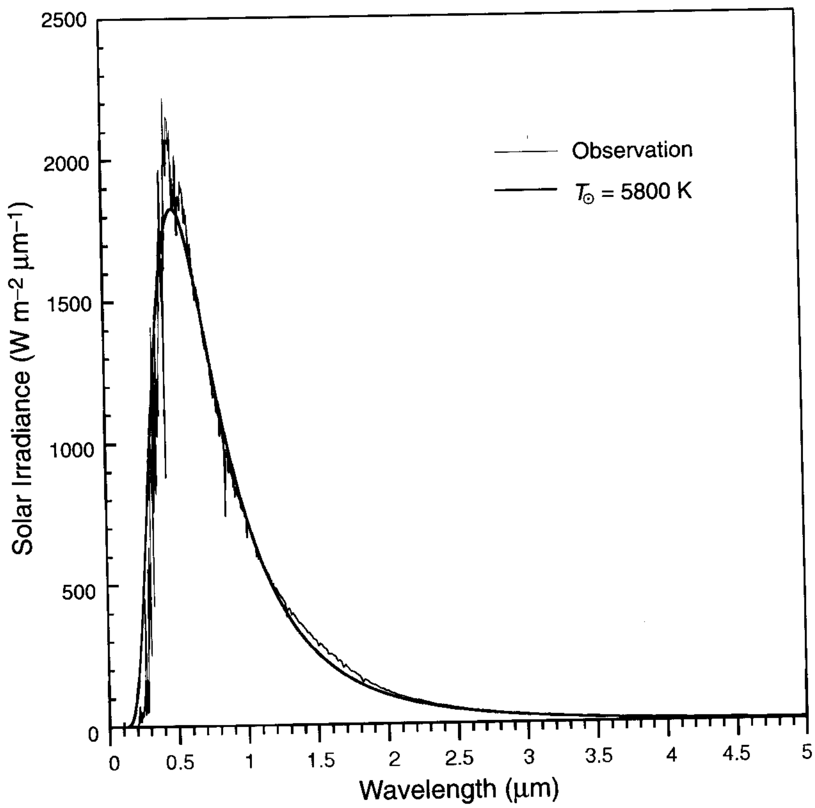


**Figure 2.9** Solar irradiance for a 50 cm$^{-1}$ spectral interval at the top of the atmosphere based on the results presented in the MODTRAN 3.7 program. Also shown is the Planck flux with a temperature of 5800 K accounting for the mean distance between the earth and the sun.

Figure 2.9 shows the spectral solar irradiance observation at the top of the atmosphere averaged over a 50 cm$^{-1}$ spectral interval as a function of wavelength up to 5 $\mu$m, based on the results presented in the MODTRAN 3.7 program (Anderson *et al.*, 1995). Although the total solar irradiance derived from this program is 1373 W m$^{-2}$, the spectral solar irradiance curve presented here is scaled with respect to the recently proposed solar constant of 1366 W m$^{-2}$ (see Section 2.3.3 for further discussion). A 50 cm$^{-1}$ spectral average has been performed to smooth out the rapid fluctuations produced by the absorption/emission line structure. However, some variabilities can still be seen, particularly in the ultraviolet spectrum. Also shown is the Planck curve with an emitting temperature of 5800 K, taking into account the mean distance between the sun and the earth. This temperature appears to fit closely with the visible and infrared spectrum characteristic of radiation emitted from the photosphere. For atmospheric applications, it is critically important to have reliable spectral solar irradiances for use in radiative transfer models. Table 2.3 gives tabulated data from 0.2 to 5 $\mu$m with

**Table 2.3**

Distribution of Solar Spectral Irradiance $S_\lambda$ from 0.2 to 100 $\mu$m in Terms of the Accumulated Energy and Percentage Based on the Values Listed in the MODTRAN 3.7 Program[a]

| $\lambda$ ($\mu$m) | $S_\lambda$ (W m$^{-2}$ $\mu$m$^{-1}$) | $S_{0-\lambda}$ (W m$^{-2}$) | $S_{0-\lambda}$ (%) | $\lambda$ ($\mu$m) | $S_\lambda$ (W m$^{-2}$ $\mu$m$^{-1}$) | $S_{0-\lambda}$ (W m$^{-2}$) | $S_{0-\lambda}$ (%) |
|---|---|---|---|---|---|---|---|
| 0.20 | 2.0832E+01 | 2.08317E+00 | 0.15250 | 3.8 | 1.0564E+01 | 1.35239E+03 | 99.00390 |
| 0.30 | 5.4765E+02 | 5.68479E+01 | 4.16163 | 3.9 | 9.6162E+00 | 1.35335E+03 | 99.07430 |
| 0.40 | 1.4042E+03 | 1.97272E+02 | 14.44155 | 4.0 | 8.6980E+00 | 1.35422E+03 | 99.13797 |
| 0.50 | 1.9619E+03 | 3.93464E+02 | 28.80410 | 4.1 | 7.9180E+00 | 1.35502E+03 | 99.19593 |
| 0.60 | 1.7632E+03 | 5.69780E+02 | 41.71153 | 4.2 | 7.2072E+00 | 1.35574E+03 | 99.24870 |
| 0.70 | 1.4300E+03 | 7.12778E+02 | 52.17994 | 4.3 | 6.5062E+00 | 1.35639E+03 | 99.29633 |
| 0.80 | 1.1257E+03 | 8.25347E+02 | 60.42075 | 4.4 | 5.7954E+00 | 1.35697E+03 | 99.33875 |
| 0.90 | 8.8835E+02 | 9.14182E+02 | 66.92404 | 4.5 | 5.2622E+00 | 1.35749E+03 | 99.37727 |
| 1.00 | 7.2943E+02 | 9.87125E+02 | 72.26392 | 4.6 | 4.8180E+00 | 1.35798E+03 | 99.41255 |
| 1.10 | 5.8743E+02 | 1.04587E+03 | 76.56425 | 4.7 | 4.4724E+00 | 1.35842E+03 | 99.44529 |
| 1.20 | 4.8921E+02 | 1.09479E+03 | 80.14558 | 4.8 | 4.1565E+00 | 1.35884E+03 | 99.47573 |
| 1.30 | 4.0851E+02 | 1.13564E+03 | 83.13614 | 4.9 | 3.8504E+00 | 1.35922E+03 | 99.50391 |
| 1.40 | 3.4450E+02 | 1.17009E+03 | 85.65813 | 5.0 | 3.5740E+00 | 1.35958E+03 | 99.53008 |
| 1.50 | 2.9066E+02 | 1.19916E+03 | 87.78592 | 6.0 | 1.8385E+00 | 1.36303E+03 | 99.78240 |
| 1.60 | 2.4644E+02 | 1.22380E+03 | 89.58999 | 7.0 | 1.0108E+00 | 1.36404E+03 | 99.85639 |
| 1.70 | 2.0453E+02 | 1.24425E+03 | 91.08726 | 8.0 | 5.9672E−01 | 1.36464E+03 | 99.90007 |
| 1.80 | 1.6829E+02 | 1.26108E+03 | 92.31927 | 9.0 | 3.7458E−01 | 1.36501E+03 | 99.92751 |
| 1.90 | 1.3725E+02 | 1.27481E+03 | 93.32404 | 10.0 | 2.4702E−01 | 1.36526E+03 | 99.94559 |
| 2.00 | 1.1624E+02 | 1.28643E+03 | 94.17501 | 11.0 | 1.6932E−01 | 1.36543E+03 | 99.95798 |
| 2.10 | 9.7416E+01 | 1.29617E+03 | 94.88816 | 12.0 | 1.2005E−01 | 1.36555E+03 | 99.96677 |
| 2.20 | 8.2132E+01 | 1.30439E+03 | 95.48942 | 13.0 | 8.7276E−02 | 1.36563E+03 | 99.97315 |
| 2.30 | 6.9594E+01 | 1.31134E+03 | 95.99889 | 14.0 | 6.5062E−02 | 1.36570E+03 | 99.97792 |
| 2.40 | 5.9198E+01 | 1.31726E+03 | 96.43226 | 15.0 | 4.9463E−02 | 1.36575E+03 | 99.98154 |
| 2.50 | 5.1023E+01 | 1.32237E+03 | 96.80577 | 16.0 | 3.8307E−02 | 1.36579E+03 | 99.98434 |
| 2.60 | 4.4280E+01 | 1.32679E+03 | 97.12994 | 17.0 | 3.0112E−02 | 1.36582E+03 | 99.98655 |
| 2.70 | 3.8672E+01 | 1.33066E+03 | 97.41305 | 18.0 | 2.3991E−02 | 1.36584E+03 | 99.98831 |
| 2.80 | 3.3815E+01 | 1.33404E+03 | 97.66058 | 19.0 | 1.9351E−02 | 1.36586E+03 | 99.98973 |
| 2.90 | 2.9589E+01 | 1.33700E+03 | 97.87720 | 20.0 | 1.5797E−02 | 1.36588E+03 | 99.99088 |
| 3.00 | 2.6133E+01 | 1.33962E+03 | 98.06850 | 30.0 | 3.4388E−03 | 1.36598E+03 | 99.99860 |
| 3.10 | 2.3093E+01 | 1.34193E+03 | 98.23756 | 40.0 | 1.0465E−03 | 1.36599E+03 | 99.99937 |
| 3.20 | 2.0476E+01 | 1.34397E+03 | 98.38746 | 50.0 | 4.2098E−04 | 1.36600E+03 | 99.99968 |
| 3.30 | 1.8186E+01 | 1.34579E+03 | 98.52059 | 60.0 | 2.0151E−04 | 1.36600E+03 | 99.99983 |
| 3.40 | 1.6191E+01 | 1.34741E+03 | 98.63913 | 70.0 | 1.0860E−04 | 1.36600E+03 | 99.99991 |
| 3.50 | 1.4562E+01 | 1.34887E+03 | 98.74574 | 80.0 | 6.3779E−05 | 1.36600E+03 | 99.99995 |
| 3.60 | 1.3032E+01 | 1.35017E+03 | 98.84114 | 90.0 | 3.9985E−05 | 1.36600E+03 | 99.99998 |
| 3.70 | 1.1670E+01 | 1.35134E+03 | 98.92657 | 100.0 | 2.6459E−05 | 1.36600E+03 | 100.0000 |

[a] The solar constant is taken to be 1366 W m$^{-2}$.

a 0.1-$\mu$m spectral interval. From 5 to 100 $\mu$m, solar irradiance accounts for about 6 W m$^{-2}$. Based on these values, about 50% of the total solar irradiance lies in wavelengths longer than the visible, about 40% in the visible region, and about 10% in wavelengths shorter than the visible. Note that from 3.5 to 5 $\mu$m, the emitted thermal infrared radiation from the earth and the atmosphere system becomes significant.

According to solar flux observations, the ultraviolet region (<0.4 $\mu$m) of the solar spectrum deviates greatly from the visible and infrared regions in terms of

Terms of the Accumulated Energy and
DTRAN 3.7 Program[a]

| $S_\lambda$ ($m^{-2}\ \mu m^{-1}$) | $S_{0-\lambda}$ ($W\ m^{-2}$) | $S_{0-\lambda}$ (%) |
|---|---|---|
| 564E+01 | 1.35239E+03 | 99.00390 |
| 162E+00 | 1.35335E+03 | 99.07430 |
| 980E+00 | 1.35422E+03 | 99.13797 |
| 180E+00 | 1.35502E+03 | 99.19593 |
| 072E+00 | 1.35574E+03 | 99.24870 |
| 062E+00 | 1.35639E+03 | 99.29633 |
| 954E+00 | 1.35697E+03 | 99.33875 |
| 622E+00 | 1.35749E+03 | 99.37727 |
| 180E+00 | 1.35798E+03 | 99.41255 |
| 724E+00 | 1.35842E+03 | 99.44529 |
| 565E+00 | 1.35884E+03 | 99.47573 |
| 504E+00 | 1.35922E+03 | 99.50391 |
| 740E+00 | 1.35958E+03 | 99.53008 |
| 385E+00 | 1.36303E+03 | 99.78240 |
| 108E+00 | 1.36404E+03 | 99.85639 |
| 672E−01 | 1.36464E+03 | 99.90007 |
| 458E−01 | 1.36501E+03 | 99.92751 |
| 702E−01 | 1.36526E+03 | 99.94559 |
| 932E−01 | 1.36543E+03 | 99.95798 |
| 005E−01 | 1.36555E+03 | 99.96677 |
| 276E−02 | 1.36563E+03 | 99.97315 |
| 062E−02 | 1.36570E+03 | 99.97792 |
| 463E−02 | 1.36575E+03 | 99.98154 |
| 307E−02 | 1.36579E+03 | 99.98434 |
| 112E−02 | 1.36582E+03 | 99.98655 |
| 991E−02 | 1.36584E+03 | 99.98831 |
| 351E−02 | 1.36586E+03 | 99.98973 |
| 797E−02 | 1.36588E+03 | 99.99088 |
| 388E−03 | 1.36598E+03 | 99.99860 |
| 465E−03 | 1.36599E+03 | 99.99937 |
| 098E−04 | 1.36600E+03 | 99.99968 |
| 151E−04 | 1.36600E+03 | 99.99983 |
| 860E−04 | 1.36600E+03 | 99.99991 |
| 779E−05 | 1.36600E+03 | 99.99995 |
| 985E−05 | 1.36600E+03 | 99.99998 |
| 459E−05 | 1.36600E+03 | 100.0000 |

r irradiance accounts for about
tal solar irradiance lies in wave-
sible region, and about 10% in
.5 to 5 $\mu$m, the emitted thermal
system becomes significant.
iolet region (<0.4 $\mu$m) of the
d infrared regions in terms of



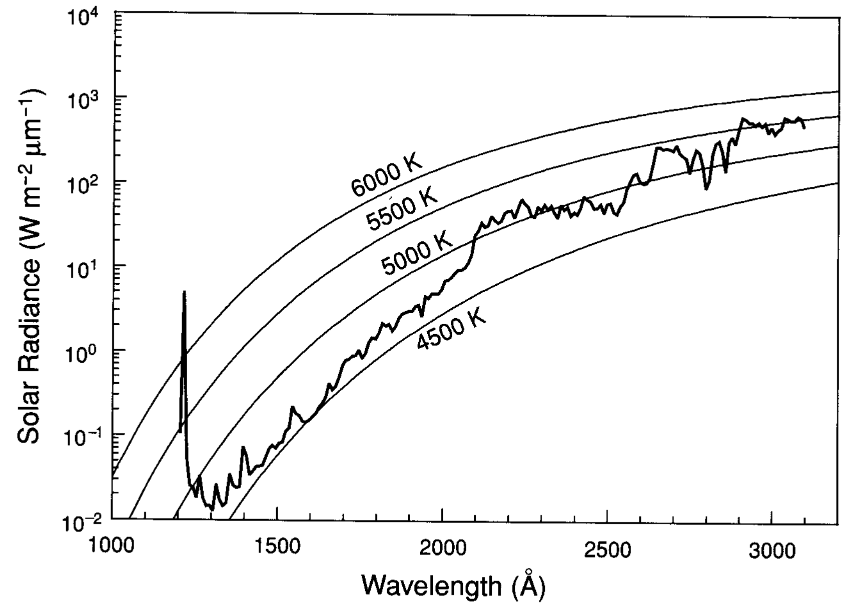


**Figure 2.10** Observed irradiance outside the earth's atmosphere in the ultraviolet region (data taken from Brasseur and Simon, 1981) and comparison with the Planck curves for temperatures ranging from 4500 K to 6000 K.

the equivalent blackbody temperature of the sun. Figure 2.10 illustrates a detailed observed solar spectrum from about 1000 to 3000 Å, along with blackbody temperatures of 4500, 5000, 5500, and 6000 K. In the interval 2100–3000 Å, the equivalent blackbody temperature of the sun lies somewhat above 5000 K. It falls gradually to a minimum level of about 4700 K at about 1400 Å. From there toward shorter wavelengths, a larger amount of energy flux is observed at the Lyman $\alpha$ emission line of 1216 Å associated with the transition of the first excited and ground states of hydrogen atoms. The ultraviolet portion of the solar spectrum below 3000 Å contains a relatively small amount of energy. However, because the ozone and the molecular and atomic oxygen and nitrogen in the upper atmosphere absorb all this energy, it represents the prime source of the energy in the atmosphere above 10 km.

## 2.3.2 Determination of the Solar Constant: Ground-Based Method

For historical reasons, we shall first introduce the ground-based method for the determination of the solar constant. Ground-based observations of solar irradiance for the purpose of determining the solar constant require three primary instruments. These are the *pyrheliometer,* the *pyranometer,* and the *spectrobolometer*. The pyrheliometer is used to measure the direct, plus some diffuse, solar radiation, while the pyranometer, utilizing a suitable shield to block the direct solar radiation from striking the instrument, measures only the diffuse solar radiation for arriving at a pyrheliometer correction. The amount of direct sunlight can then be calculated by subtracting the flux density measured by the pyranometer from that measured by the pyrheliometer. The spectrobolometer is a combination of a spectrograph and a coelostat. A coelostat is a mirror that follows the sun and focuses its rays continuously on the entrance slit of the spectrograph, which disperses the solar radiation into different wavelengths by means of a prism or diffraction grating. In the Smithsonian solar constant measurements, about 40 standard wavelengths between 0.34 and 2.5 $\mu$m are measured nearly simultaneously from the record of the spectrograph. The instrument for these measurements is called a *bologram*. There are two techniques of measuring the solar constant from the ground-based radiometer, called the *long* and *short* methods of the Smithsonian Institution. The long method is more fundamental and establishes the basis for the short method. The long method uses the Beer–Bouguer–Lambert law and is introduced in the following.

Consider an atmosphere consisting of plane-parallel layers. At a given position of the sun, which is denoted by the solar zenith angle $\theta_0$, the effective path length of the air mass is $u \sec \theta_0$, where

$$u = \int_{z_1}^{z_\infty} \rho dz. \tag{2.3.1}$$

In this equation $z_1$ is the height of the station and $z_\infty$ denotes the top of the atmosphere. On the basis of the Beer–Bouguer–Lambert law, the irradiance $F$ of the direct solar radiation of wavelength $\lambda$ observed at the surface level is given by

$$F_\lambda = F_{\lambda 0} \exp(-k_\lambda u \sec \theta_0) = F_{\lambda 0} T_\lambda^m, \tag{2.3.2}$$

where $F_{\lambda 0}$ is the monochromatic solar irradiance at the top of the atmosphere, $k_\lambda$ denotes the monochromatic mass extinction cross section, $T_\lambda$ is the monochromatic transmissivity defined in Eq. (1.4.10), and $m$ ($= \sec \theta_0$) represents the ratio of the air mass between the sun and the observer to the air mass with respect to the local zenith distance. Upon taking the logarithm, we find

$$\ln F_\lambda = \ln F_{\lambda 0} + m \ln T_\lambda. \tag{2.3.3}$$

Observations of $F_\lambda$ may be made for several zenith angles during a single day. If the atmospheric properties do not change during the observation period, then the transmissivity $T_\lambda$ is constant. A plot of ln $F_\lambda$ versus $m$ shown in Fig. 2.11 may be extrapolated to the zero point, which represents the top of the atmosphere ($m = 0$). This is referred to as the *Langley plot*. If observations of the monochromatic irradiance are carried out for wavelengths covering the entire solar spectrum, then we have

$$F_\odot = \int_0^\infty F_{\lambda 0} d\lambda \approx \sum_{i=1}^{N} F_{\lambda_i 0} \Delta\lambda_i, \tag{2.3.4}$$

where $N$ is the total number of the monochromatic irradiances measured. The irradiance $F_\odot$ corresponds to the actual distance between the earth and the sun, $r$. By using

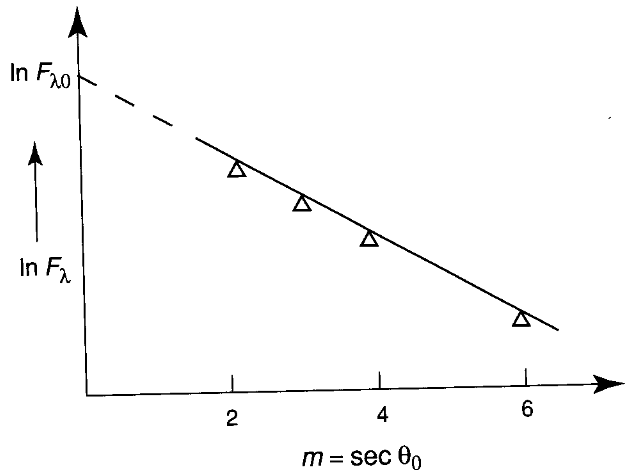


**Figure 2.11** Hypothetical observed monochromatic solar irradiances $F_\lambda$ as a function of the effective path length from which the solar irradiance at the top of the atmosphere can be graphically determined, referred to as the Langley plot.

the mean distance $r_0 = a$, the solar constant is defined by

$$S = F_\odot (r/a)^2. \tag{2.3.5}$$

The foregoing outlines the theoretical procedures of the Smithsonian long method for the determination of the solar constant. However, the atmosphere is essentially opaque for wavelengths shorter and longer than about 0.34 $\mu$m and 2.5 $\mu$m, respectively. Consequently, flux density observations cannot be made in these regions. Therefore, empirical corrections are needed for the omitted ranges, which account for about 8% of the solar flux.

There are other sources of error inherent in the Smithsonian long method caused by (1) empirical corrections for the absorption of ultraviolet by ozone, and the absorption of infrared by water vapor and carbon dioxide in the wings of the solar spectrum; (2) an unknown amount of diffuse radiation entering the aperture of the observing instrument; (3) variations of $k_\lambda$ and the possible effects of aerosols during a series of measurements; and (4) measurement errors. Therefore, in spite of careful evaluation and observation, a certain amount of error is inevitable.

Employing the Smithsonian long method, each determination requires about 2 to 3 hours of observation time, plus twice that much time for the data reduction. In addition, there is no assurance that atmospheric properties and solar conditions will remain unchanged during the observation period. Because of this uncertainty and the burdensome, time-consuming work involved, a short method was devised to determine the solar constant.

In the short method, the diffuse component of solar radiation (the sky brightness) is measured for a given locality over a long period of time, so that a mean diffuse intensity can be determined. Thus, a pyranometer reading of diffuse solar radiation will differ from the mean by an amount $\varepsilon$, called the *pyranometer excess*. In reference to Section 1.1.4 and Fig. 3.9, the attenuation of solar radiation on a clear day is due to scattering by molecules and aerosol particles, and absorption by various gases, primarily water vapor. If total precipitable water is given by $w$, an empirical relationship between the attenuation of direct solar irradiance and scattering and absorption effects may be expressed in the form $F_\lambda = w + q_\lambda \varepsilon$, where $q_\lambda$ is a constant empirically determined for each wavelength for a given locality. With $q_\lambda$ known, the spectral value of the solar irradiance can be found from the observed precipitable water and a pyranometer reading.

On the basis of a long series of previous observations of $F_\lambda$, $m$, and $T_\lambda$ at a given location where the solar constant measurement has been made, a graph of $F_\lambda$ versus air mass $m$ can be constructed for a set value of $T_\lambda$. Thus, for a particular measurement of $F_\lambda$ with a known air mass $m$, the corresponding transmissivity $T_\lambda$ can be found from the graph. Once $T_\lambda$ has been determined, solar irradiance at the top of the atmosphere $F_{0\lambda}$ can be evaluated through Eq. (2.3.2). After this point, evaluation of the solar constant proceeds in the same manner as in the long method. In the short method, the required measurements include a bologram of the sun, an observation of sky brightness by the pyranometer, and air mass determined by the position of the sun from a theodolite. These three measurements take only about 10 to 15 minutes. From the thousands of observations at various locations around the world during a period of more than half a century, the best value of the solar constant determined by the Smithsonian methods is 1353 W m$^{-2}$.

The presence of aerosols in the atmosphere imposes limitations on the accuracy of ground-based radiometric measurements of the solar constant (see, e.g., Reagan *et al.*, 1986). To minimize atmospheric effects, a number of measurements have also been made in the upper atmosphere and outer space. These have included observations made from balloons floating in the 27- to 35-km altitude range, jet aircraft at about 12 km, the X-15 rocket aircraft at 82 km, and the Mars Mariner VI and VII spacecrafts entirely outside the atmosphere. The solar constant derived from these experiments varies. Based on a series of measurements from high-altitude platforms, a standard solar constant of 1353 ($\pm$21) W m$^{-2}$ was issued in 1976 by the National Aeronautics and Space Administration (Thekaekara, 1976).

### 2.3.3 Satellite Measurements of the Solar Constant

Measurements of incoming solar irradiance have been routinely made from satellite platforms since the mid-1970s. However, the high-accuracy, high-stability satellite-borne radiometer was only developed and incorporated in the Nimbus 7 satellite in 1978. This radiometer was an electrically calibrated cavity radiometer. The basic concept of blackbody cavity radiation was shown in Fig. 1.6. Radiometers of this design for use in satellites had a black painted cavity that absorbed nearly all the solar radiation impinging on it. The absorbed radiation raised the temperature of the cavity so that a radiant power could be measured corresponding to the increase in temperature. Such a cavity can also be heated by an electrical element in a manner equivalent to the incident sunlight. Because the input electrical power can be measured accurately, the temperature response of the radiometer can be calibrated, and it is thus referred to as the *self-calibrating radiometer*.

Solar constant data have been derived from total solar irradiance measurements made by self-calibrating radiometers aboard a number of satellites since 1978. These include the Nimbus 7 Earth Radiation Budget (ERB) mission in 1978; the Solar Maximum Mission (SMM) Active Cavity Radiometer Irradiance Monitor 1 (ACRIM I) in 1980; the Earth Radiation Budget Experiment (ERBE) on board the NASA Earth Radiation Budget Satellite (ERBS, 1984), NOAA 9 (1984), and NOAA 10 (1986); and the ACRIM II measurements on board the Upper Atmosphere Research Satellite (UARS, 1991). Figure 2.12 shows the daily measurements of the solar constant from these satellites from 1979 to 1996. The solid lines are 81-day running means of the daily data. The absolute radiance scale of the ACRIM II data has been adjusted to

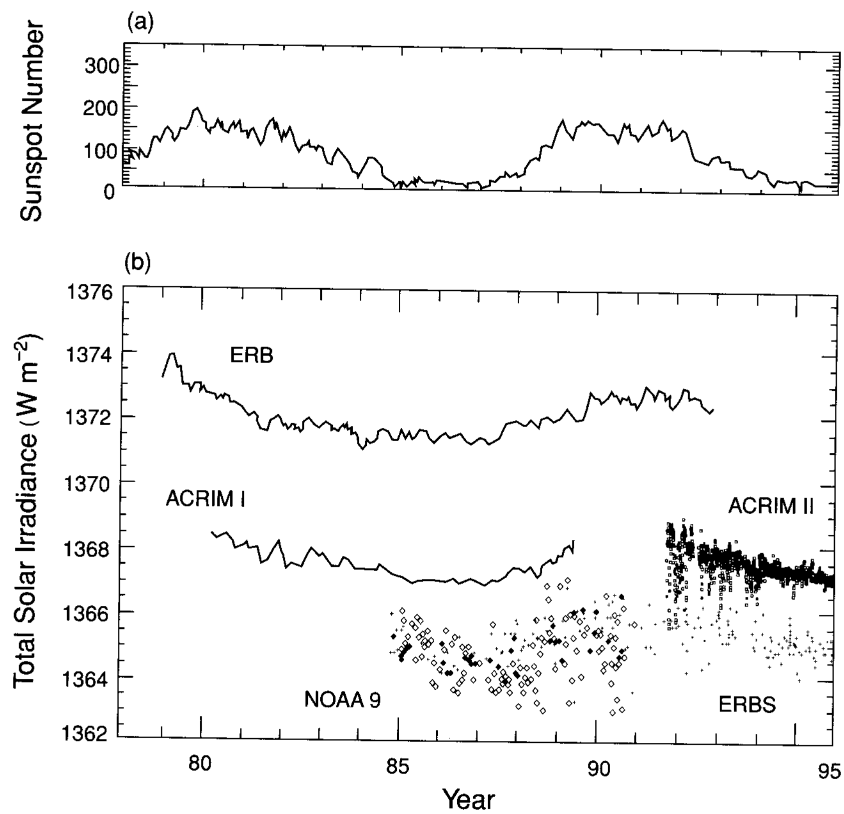


**Figure 2.12** Solar activity variations from 1978 to 1996 illustrated by (a) the sunspot number and (b) changes in total solar irradiance. The results were obtained from the ERB radiometer on the Nimbus-7 satellite, ACRIM I on the Solar Maximum Mission (SMM) satellite, ACRIM II on the UARS, and the ERBE program (NOAA-9 and ERBS). The solid lines are 81-day running means of the daily data. Total solar irradiance increases during times of maximum solar activity relative to its levels in the intervening activity minimum. The differences in absolute irradiance levels among various measurements are of instrumental origin (data taken from Lean and Rind, 1998).

match the results of ACRIM I. The differences in absolute irradiance levels among various measurements depicted in this figure are attributed to the instrument sensitivity changes related to temperature or aspect drifts. In particular, ERB and ERBS data differed by about 10 watts per square meter. The top panel shows the sunspot numbers over the same period. It is quite clear that the data displayed in Fig. 2.12 provide irrefutable evidence of the 11-year solar constant cycle. When solar activity is high, as indicated by the sunspot number, the total and UV radiative outputs from the sun increase. Dark sunspots on the solar disk reduce total radiative output because their emission is less than that of the surrounding disk. However, after sunspots develop, magnetic regions involving faculae and plages where emission is enhanced also increase. These regions are evident as complexes of bright emission. The sun's irradiance fluctuates because radiation sources are not homogeneously distributed on its disk. Magnetic fields erupting from the solar convection zone (Section 2.1) into the overlying solar atmosphere generate active regions and complexes in which the local radiation is altered relative to the background solar disk. Magnetic activity erupts, evolves, and decays at different rates throughout the 11-year cycle, generating sunspots, plages, and faculae that modulate total and spectral solar radiative outputs. Finally, it should be noted that our knowledge of the 11-year irradiance cycle is imperfect because of uncertainties arising from the limited duration of space-borne solar monitoring that barely exceeds one 11-year cycle, as well as instrumental uncertainties that cause variable signals in individual satellite solar radiometers.

A number of analyses of the mean total solar irradiance have been reported. Based on the analysis of the solar irradiance measurements taken by the cavity sensor in a number of the satellites depicted in Fig. 2.12, a mean value for the solar constant of 1366 W $m^{-2}$ with a measurement uncertainty of $\pm 3$ W $m^{-2}$ has been suggested (Lean and Rind, 1998). The solar constant value is critical in the interpretation of measured solar absorption and heating rates in the atmosphere.

## Exercises

2.1 Compute the solar elevation angle at solar noon at the poles, 60° N(S), 30° N(S), and the equator. Also compute the length of the day (in terms of hours) at the equator and at 45° N at the equinox and solstice.

2.2 From the geometry of an ellipse and the equation defining it, derive Kepler's first law denoted in Eq. (2.2.5).

2.3 Based on the conservation of angular momentum that the radius vector drawn from the sun to the planet sweeps out equal areas in equal time, derive Kepler's second law denoted in Eq. (2.2.6).

2.4 (a) Derive Kepler's third law by equating Newton's law of universal gravitation and the centrifugal force required to keep the planet in a circular orbit. (b) Given that the NOAA polar satellites orbit at about 850 km above the earth's surface, what would be the period of these satellites? (c) Geostationary satellites have the same angular velocity as the earth. What would be the required height for these satellites?

2.5 Given the solar co
$150 \times 10^6$ km, and t
temperature of the s

2.6 If the average outpu
is $6.37 \times 10^3$ km, w
one day?

2.7 Compute the fractio

2.8 Consider a circular
infinitely thin black
emit toward the eart
centimeter of the ea
over the receiving s

2.9 Assume that $\bar{r}$ is the
amount of flux refle
atmosphere system
the earth–atmosphe

2.10 The following tabl
their albedos. Emp
temperatures of the

2.11 The height of ear
GOES satellites, is
1.2, calculate the e
system, assuming
and assuming that

2.12 Show that the cha
earth–sun distance
and the sun varies
and July 5, respect
temperature.

2.13 Calculate the dail
at the winter solst
earth–sun distance
in Fig. 2.8.

2.14 Prove that annual insolation is the same for corresponding latitudes in the two hemispheres [you may use the results in Eqs. (2.2.23) and (2.2.24) for analysis].

2.15 Show that the difference between the length of summer and that of winter is given by $\widetilde{T}4e \sin \omega/\pi$. In carrying out this exercise, first define the length using the astronomical season definition and then utilize Kepler's expressions by approximation.

2.16 Reproduce the daily solar insolation graph presented in Fig. 2.8 using Eqs. (2.2.21), (2.2.9), and (2.2.10).

2.17 Compute and plot the solar irradiance at the top of the earth's atmosphere emitted from temperatures of 5000, 5500, and 6000 K. Compare your results with those presented in Figs. 2.9 and 2.10.

2.18 On a clear day, measurements of the direct solar flux density $F$ at the earth's surface in the 1.5- to 1.6-$\mu$m wavelength interval give the following values:

| Zenith angle (degree): | 40° | 50° | 60° | 70° |
|---|---|---|---|---|
| $F$ (W m$^{-2}$): | 13.95 | 12.55 | 10.46 | 7.67 |

Find the solar flux density at the top of the atmosphere and the transmissivity of the atmosphere for normal incidence [see Eq. (1.4.10)] in this wavelength interval.

## Suggested Reading


Berger, A. L. (1988). Milankovich theory and climate. *Rev. Geophys.* **26,** 624–657. This paper offers an authoritative overview of contemporary theory of the earth's orbit about the sun and its impact on climate.

Coulson, K. L. (1975). *Solar and Terrestrial Radiation.* Academic Press, New York. Chapters 3 and 4 give a comprehensive illustration of various kinds of pyrheliometers and pyranometers.

Hoyt, D. V., and Schatten, K. H. (1997). *The Role of the Sun in Climate Change.* Oxford University Press, New York. Chapters 2 and 3 contain a readable discussion of the composition of the sun and the solar constant from a historical perspective.

Jastrow, R., and Thompson, M. H. (1984). *Astronomy: Fundamentals and Frontiers,* 2nd ed. Wiley, New York. Chapter 12 provides an in-depth discussion and delightful photos of the structure and composition of the sun.

Lean, J., and Rind, D. (1998). Climate forcing by changing solar radiation. *J. Climate* **11,** 3069–3094. This paper includes a comprehensive and authoritative review of the solar constant and solar spectrum measurements and variabilities.


# Chapter 3

## 3.1 Composition an

It is now generally accep
solid materials that cond
The earth's present atm
generated from volatile
which the earth formed.
lost because the cosmic
which contains about 9(
The heavy bombardmen
extant by 3.5 BY, at whi
The post-heavy bombar
with traces of CO and H
sphere, associated with
on the earth's surface. A
have evolved to compen
suggested that the biota
consequence of photosy
naturally. The major inc
The level of free $O_2$ is a
layer that provided an ef
we define the region of

### 3.1.1 Thermal Struc

To describe the interacti
understand the atmosph
the region of the atmos
light, we first present t
which is shown in Fig
latitude regions. Accord
Union of Geodesy and

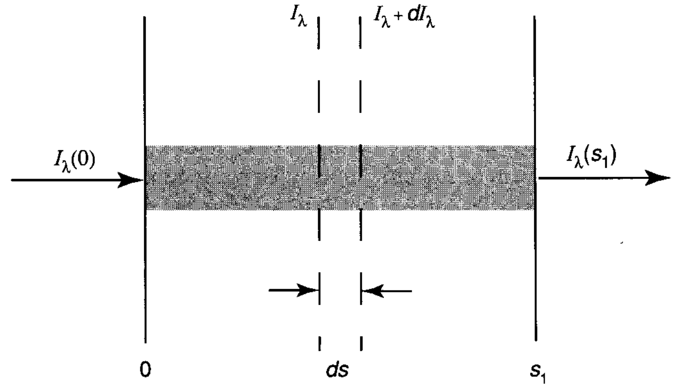


**Figure 1.13** Depletion of the radiant intensity in traversing an extinction medium.

In this manner, the source function has units of radiant intensity. It follows that Eq. (1.4.3) may be rearranged to yield

$$\frac{dI_\lambda}{k_\lambda \rho\, ds} = -I_\lambda + J_\lambda. \tag{1.4.5}$$

This is the general radiative transfer equation without any coordinate system imposed, which is fundamental to the discussion of any radiative transfer process.

### 1.4.2 Beer–Bouguer–Lambert Law

Consider a direct light beam from the sun, which covers the wavelengths from about 0.2 to 5 $\mu$m. Emission contributions from the earth–atmosphere system can be generally neglected, as discussed in Section 1.2. Moreover, if the diffuse radiation produced by multiple scattering can be neglected, then Eq. (1.4.5) reduces to the following form:

$$\frac{dI_\lambda}{k_\lambda \rho\, ds} = -I_\lambda. \tag{1.4.6}$$

Let the incident intensity at $s = 0$ be $I_\lambda(0)$. Then the emergent intensity at a distance $s$ away shown in Fig. 1.13 can be obtained by integrating Eq. (1.4.6) and is given by

$$I_\lambda(s_1) = I_\lambda(0) \exp\left(-\int_0^{s_1} k_\lambda \rho\, ds\right). \tag{1.4.7}$$

Assuming that the medium is homogeneous, so that $k_\lambda$ is independent of the distance $s$, and defining the path length

$$u = \int_0^{s_1} \rho\, ds, \tag{1.4.8}$$

Eq. (1.4.7) can be expressed by

$$I_\lambda(s_1) = I_\lambda(0) e^{-k_\lambda u}. \tag{1.4.9}$$

This is known as Beer's law or Bouguer's law or Lambert's law, referred to here as the Beer–Bouguer–Lambert law, which states that the decrease in the radiant intensity traversing a homogeneous extinction medium is in accord with the simple exponential function whose argument is the product of the mass extinction cross section and the path length. Since this law involves no directional dependence, it is applicable not only to the intensity quantity but also to the flux density and the flux.

From Eq. (1.4.9), we can define the monochromatic transmissivity $T_\lambda$ as follows:

$$T_\lambda = I_\lambda(s_1)/I_\lambda(0) = e^{-k_\lambda u}. \tag{1.4.10}$$

Moreover, for a nonscattering medium, the monochromatic absorptivity, representing the fractional part of the incident radiation that is absorbed by the medium, is given by

$$A_\lambda = 1 - T_\lambda = 1 - e^{-k_\lambda u}. \tag{1.4.11}$$

Equations (1.4.10) and (1.4.11) are normally expressed in the wavenumber domain in conjunction with the application of infrared radiation transfer. Finally, if there is a scattering contribution from the medium, certain portions of the incident radiation may reflect back to the incident direction. In this case, we may define the monochromatic reflectivity $R_\lambda$, which is the ratio of the reflected (backscattered) intensity to the incident intensity. On the basis of the conservation of energy, we must have

$$T_\lambda + A_\lambda + R_\lambda = 1 \tag{1.4.12}$$

for the transfer of radiation through a scattering and absorbing medium.

### 1.4.3 Schwarzschild's Equation and Its Solution

Consider a nonscattering medium that is in local thermodynamic equilibrium. A beam of intensity $I_\lambda$ passing through it will undergo the absorption and emission processes simultaneously. This is the case for the transfer of thermal infrared radiation emitted from the earth and the atmosphere. The source function, as defined in Eq. (1.4.4), is given by the Planck function and can be expressed by

$$J_\lambda = B_\lambda(T). \tag{1.4.13}$$

Hence, the equation of radiative transfer can now be written as

$$\frac{dI_\lambda}{k_\lambda \rho\, ds} = -I_\lambda + B_\lambda(T), \tag{1.4.14}$$

where $k_\lambda$ is now the absorption coefficient. The first term in the right-hand side of Eq. (1.4.14) denotes the reduction of the radiant intensity due to absorption, whereas the second term represents the increase in the radiant intensity arising from blackbody emission of the material. To seek a solution for Schwarzschild's equation, we define the monochromatic optical thickness of the medium between points $s$ and $s_1$ as shown